

# Engineering morphogenesis of cell clusters with differentiable programming

Ramya Deshpande,<sup>1,\*</sup> Francesco Mottes,<sup>1,2,\*</sup> Ariana-Dalia Vlad,<sup>3</sup> Michael P. Brenner,<sup>1</sup> and Alma dal Co<sup>2</sup>

<sup>1</sup>*School of Engineering and Applied Sciences, Harvard University, Cambridge MA 02138*

<sup>2</sup>*Department of Computational Biology, University of Lausanne, Lausanne, Switzerland*

<sup>3</sup>*Harvard College, Cambridge, MA 02138*

(Dated: September 24, 2024)

Understanding the rules underlying organismal development is a major unsolved problem in biology. Each cell in a developing organism responds to signals in its local environment by dividing, excreting, consuming, or reorganizing, yet how these individual actions coordinate over a macroscopic number of cells to grow complex structures with exquisite functionality is unknown. Here we use recent advances in automatic differentiation to discover local interaction rules and genetic networks that yield emergent, systems-level characteristics in a model of development. We consider a growing tissue with cellular interactions mediated by morphogen diffusion, differential cell adhesion and mechanical stress. Each cell has an internal genetic network that is used to make decisions based on the cell's local environment. We show that one can simultaneously learn parameters governing the cell interactions and the genetic network for complex developmental scenarios, including the symmetry breaking of an embryo from an initial cell by creation of emergent chemical gradients, homogenization of growth via mechanical stress, programmed growth into a pre-specified shape, and the ability to repair from damage. When combined with recent experimental advances measuring spatio-temporal dynamics and gene expression of cells in a growing tissue, the methodology outlined here offers a promising path to unravelling the cellular bases of development.

Morphogenesis, the emergence of distinct anatomical forms from dividing cellular assemblies, hinges on the delicate coordination of diverse cellular and molecular processes across multiple spatial and temporal scales. Programming cells to achieve desired morphogenetic outcomes is extremely challenging. Unlike systems guided by centralized control signals [1], most developmental complexity arises from the interplay of local communications, sensing, and information processing within individual cells, with minimal external influence [2]. The emergent nature of collective cell phenomena, coupled with the complexity of modeling them in adequate detail, imposes severe limits to the effectiveness of computational approaches to inverse design.

Recent experimental advances offer unprecedented opportunities for morphogenetic engineering [3, 4], enabling the engineering of tailored cellular interactions, with applications ranging from population control [5] to programming multicellular assembly patterns [6]. Leveraging the intrinsic self-organizing tendencies of cell clusters has also facilitated the production of diverse organoids that mimic multiple aspects of real tissues and organs [7–9]. The ability to quantitatively guide existing self-organizing developmental programs or engineer novel ones holds significant implications for both fundamental scientific understanding and biotechnology [10, 11]. Many of these successes, however, heavily rely on manually crafted and qualitative cellular interaction rules and protocols. Heuristic experimental rules often exhibit drawbacks, including system specificity, limited robustness, and insufficient reproducibility [12]. Developing more versatile and efficient tools for biological design has

the potential to extend the reach and impact of experimental techniques.

Inverse design tasks are usually translated into optimization problems, wherein the objective is to minimize the discrepancy between a property of the simulated system state and its desired value. While sophisticated computational models of cell behavior exist [13, 14], their applicability to reverse engineering remains limited, particularly in high-dimensional parameter spaces where parameter sweeps and evolutionary searches become inefficient. Automatic differentiation (AD) algorithms, on the other hand, enable efficient calculation of sensitivities of observables with respect to input parameters. While originally developed for training large neural networks [15, 16], the same technical infrastructure can be used to differentiate through simulations of physical processes, offering gradient-based optimization as a viable alternative to tackle hard inverse problems of various scientific interest. Successful examples include the design of self-assembling materials [17], the establishment of data-driven discretizations for partial differential equations [18], nonequilibrium statistical mechanics [19] and the design of quantum devices [20]. Neural Cellular Automata [21] represented an initial demonstration of how these methods could be used to engineer collective behaviors inspired by biology in lattice models. Hiscock, instead, showed that AD could be used to successfully learn meaningful couplings in ODE models of genetic networks [22].

Here, we consider a model of a tissue composed of cells, where each cell can divide, grow, exert stress, as well as excrete and sense morphogens. Cellular decisions are made in response to the local environment, via an internal genetic network (Fig. 1). Starting from random initial parameters, we demonstrate that we can learn the pa-

---

\* These authors contributed equally to this work.

rameters governing both cellular and genetic interactions so that the cluster of cells undergoes non-trivial developmental scenarios, ranging from symmetry breaking of an embryo from a progenitor cell, to the creation of emergent chemical gradients, to homogenization of growth via chemical signalling and mechanical stress response, to programmed growth into a pre-specified shape, which is able to repair itself from damage. The framework allows for the probing of the relationship between the capabilities of individual cells and the emergent properties of the resulting tissues.

## MODEL AND OPTIMIZATION FRAMEWORK

### Forward Model

We model tissue growth using soft spheres interacting through a Morse potential [23]. We mostly consider two-dimensional systems since three-dimensional systems rapidly become too computationally intensive to optimize with our current implementation. Our methods are nonetheless applicable in principle to any physical model of cell interactions and we show some simple experiments with 3D systems. In our model, cells grow at a fixed rate until reaching a maximum radius, leading to continuous mechanical reorganization. Cells secrete  $M$  morphogens, measure local concentrations and spatial gradients of these chemicals, and sense mechanical stress. This locally sensed information guides decisions on chemical secretion modulation and division probability (Fig. 1a). Cell division events are stochastic, producing two daughter cells, each with half the volume of a fully grown mother cell. Decision-making circuits are modeled as regulatory networks comprising  $N$  interacting genes with trainable excitatory or inhibitory couplings (Fig. 1b). The regulatory network processes the information sensed by individual cells to output rates of division, chemical secretion, etc. In most examples, the regulatory network weights are shared by all cells, though we also explore one scenario where two cell types have partially different regulatory networks. Further mathematical detail can be found in the *Supplementary Information*.

### Inverse Design

Our objective is to discover local growth rules that enable cells to develop into a final configuration with desired properties. To effectively navigate the high-dimensional, non-convex parameter space of local interaction rules, we employ gradient descent schemes, widely used in modern machine learning for such optimizations. Our entire simulation is written to be automatically differentiable, leveraging recent advances from the deep learning and reinforcement learning communities. We utilize the JAX library [24] for efficient numerical and

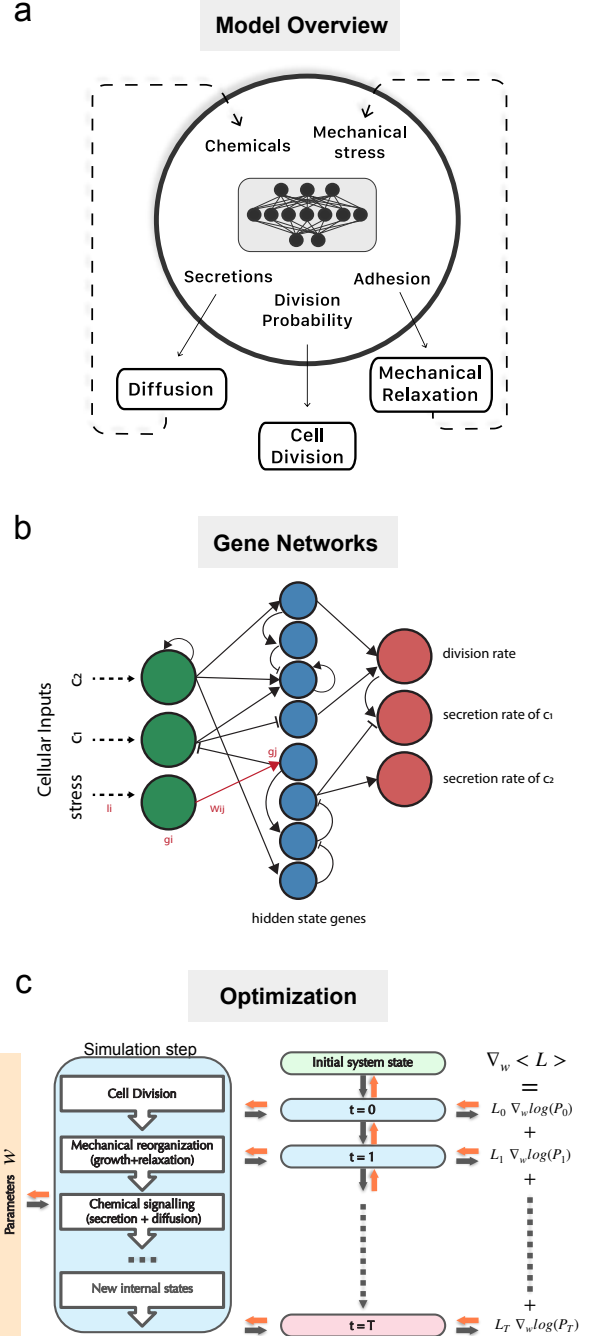


FIG. 1. **Modeling and Optimization Framework.** (a) Model overview. Decision-making circuits in cells sense local chemical and mechanical inputs to regulate secretion, division probability, and adhesion. The environment responds to cellular outputs by handling chemical diffusion, cell division, and mechanical relaxation. (b) Input signals are integrated and elaborated in each cell by internal gene regulatory networks. Green gene nodes sense inputs, blue genes are intermediates and red genes can modify cellular actions. Gene expression levels in each node are maintained from one simulation step to the next, providing memory to the system. (c) Gradient calculation and optimization. Following the REINFORCE approach, the log probability gradient of each time step is weighted by action rewards to estimate the average gradient and parameters are updated through gradient descent. Gradients flow through the whole differentiable simulation, accounting for environment contributions.

automatic differentiation algorithms, and other JAX-based libraries such as Equinox [25] and JAX-MD [26] for molecular dynamics.

We employ score-based methods such as REINFORCE [27] to address the intrinsic stochasticity of growth dynamics, which implies that the loss function is not necessarily differentiable (Fig. 1c). In the REINFORCE update, rewards and penalties are assigned to each action taken (i.e. each cell division) to provide the weighting signal for the gradient of the trajectory probability. This weighted gradient is then used to nudge the weights of the gene network in the right direction. In practice, the system gradually learns which division events are the most favorable and increases their probability for the next simulation. To guide the reader possibly unfamiliar with these concepts, we also include a set of in-depth tutorial notebooks in the GitHub repository [28] and a longer theoretical explanation in the *Supplementary Information*. Since the dynamics of the environment, including chemical secretion and diffusion, depend partly on the same parameters (the gene network couplings) that cells use to decide whether to divide or not (their “policy”), it is essential to evaluate the gradient of the environment dynamics with respect to the gene network parameters. This necessity makes automatic differentiation particularly crucial in this context. Once the necessary gradients are calculated, optimization is performed using well-established gradient descent schemes, such as Adam [29]. The learned networks are then further simplified by removing all edges with weights smaller than an experiment-dependent threshold, such that the functional backbone of pruned network be highlighted while preserving the optimized properties.

## CHEMICAL REGULATION OF CELLULAR ADHESION

The differential adhesion hypothesis posits that populations of cells can adopt specific morphologies based on differences in adhesive strength [30]. During morphogenesis, a cadherin code regulates the spatial organization of developing tissue [31, 32]. Engineered cellular circuits can use gene regulatory networks to dynamically modulate adhesion and program self-organization [6]. Here, we show that gene interactions can be learned that use chemical signaling to modulate homotypic and heterotypic adhesion to achieve a target spatial pattern in a population with different cell types.

In our model, a population of three cell types is subject to Brownian motion and interacts via a Morse pairwise potential. The well depth of the potential between a pair of cells is dictated by the concentration of homotypic and heterotypic “cadherins” in each cell. Each cell type produces its respective homotypic cadherin and a shared heterotypic cadherin, regulated by chemical signaling. Each cell type utilizes the same gene network, but can only secrete chemicals and express cadherins of its own type.

To achieve a desired spatial organization, we construct three loss functions based on pairwise distances between cells. For a lattice-like structure, we minimize the sum of pairwise distances between cells of different types (Fig 2a). To organize the structure into three lobes, we minimize the sum of pairwise distances between cells of the same type (Fig 2b). To achieve a core-shell structure, we minimize the distance of each cell to a pre-specified radius, based on the cell type (Fig 2c).

The optimization process identifies effective solutions by allowing cells to observe their own type and regulate the pairwise potential between cell types. For a lattice-like structure, cells up-regulate their heterotypic cadherin and down-regulate their homotypic cadherin. Conversely, to create a lobed structure, they up-regulate their homotypic cadherin and down-regulate their heterotypic cadherin. These patterns of homo- and heterotypic adhesion are consistent with observations from cell culture sorting experiments [31]. Achieving core-shell structures requires a more complex regulatory network (Fig 2c).

## SPATIAL CONTROL OF TISSUE GROWTH

Understanding how to program the growth of complex shapes can aid in our comprehension of developmental body plans driven by chemical patterning. Rationally designed synthetic gene circuits have already been shown to be able to drive the formation of target multicellular structures found in morphogenesis [6, 33]. We investigate here how to use our framework to discover new decision-making circuits that utilize local chemical interactions to grow pre-specified shapes. These rules are, as above, formulated as gene regulatory circuits. We focus in particular on two fundamental shapes commonly found in developmental biology: elongation and branching. The symmetry-breaking elongation process is the first geometric-defining process to happen in many developmental programs and is vital, for example, for establishing the antero-posterior axis in animals [34]. Branching is possibly the next most ubiquitous process in the development of multicellular organisms and branched structures are found from plant roots to blood vessels and mammary epithelial cultures [35].

We show below that gene regulations that achieve these final structures can be learned in our model. Notably, we also show that mechanisms optimized solely to achieve a specific final structure exhibit emergent properties that they were not explicitly trained to achieve. In particular, gene circuits learn to leverage, modify and generate chemical gradients and they display basic regenerative capabilities.

### Elongation

We consider a three dimensional model of dividing cells that we optimize to minimize the squared sum of the z-

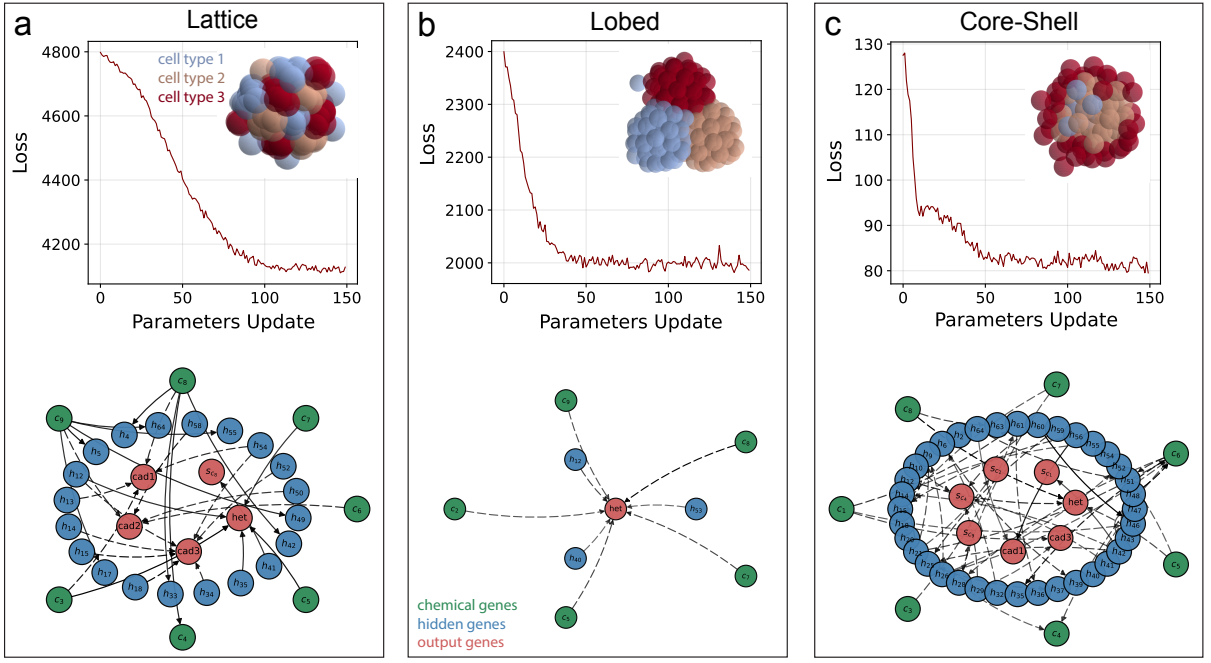


FIG. 2. **Chemical Regulation of Cellular Adhesion.** Learned chemical regulation of cellular adhesion guides the assembly of different spatial cluster arrangements. The top part of the panels show the training loss curves for three different optimization targets. The insets show the final state of a simulation after the learning, with colors denoting different cell types. The bottom sections show the learned and pruned gene network; *Cad1*, *Cad2*, and *Cad3* are the homotypic cadherins of the three cell types, and *Het* is the heterotypic cadherin expressed in all cell types. (a) Lattice-like structure. Cells are arranged to minimize the sum of pairwise distances between heterotypic cells. (b) Lobed structure. Cells minimize the sum of pairwise distances between homotypic cells. (c) Core-shell structure. Cells are arranged to minimize the distance of cells from a predefined radius, dependent on their type. The final configuration is here shown as a cross-section to highlight the internal structure.

coordinates of cells, thus requiring the cluster to elongate vertically (Fig. 3a). Local chemical concentrations, local estimated chemical gradients, cell size, and division propensities are passed as inputs into the cells' gene network (Fig. 3b), that infer positional information through local physical communication. Simulations start from a single cell and grow to a total of 120 cells.

In order to globally assume an elongated shape, cells learn to create emergent chemical gradients or control existing ones, even though this task is not included in the optimization objective (Fig 3c). The cells learn to divide primarily at one or both ends of the growing cluster. Since the cluster edge itself moves as a consequence of new cells being added, the gene networks must implement a non-trivial control mechanism to keep the cluster growing.

### Branching

We simulate the growth of a cluster from a single cell to 130 cells, restricting ourselves to the 2-dimensional case for computational simplicity. With a similar spirit to diffusion-based geometry [35], we simulate permeable diffusive boundaries between the cell cluster and the sur-

rounding implicit medium by connecting boundary cells to a ghost chemical sink node. Gene networks have access to the local chemical concentrations, estimates of local chemical gradients, their own cell radius and division propensity. They do not have access to their own absolute spatial coordinates.

To learn more complex branched structures, we construct a position-based shape loss. At each time point, cell divisions that place cells within the region designating the desired shape are assigned a reward, the others a penalty. In this case, we impose a V-shaped spatial reward structure (Fig. 4a on the right) augmented with an asymmetry penalty on the x-coordinate, in order to promote the growth of both arms at the same time. Also in this case, a variety of chemical patterns emerge in the learned simulation (Fig 4b), and the cluster learns to divide cells primarily at the tips of the branching structure. Clusters visually acquire a branched shape, even when simulated for 500 cell divisions more than optimized for. While shape errors clearly emerge, they do mostly in the form of smaller branches that begin to sprout from the main branched structure (Fig 4c). Furthermore, the learned network displays emergent regenerative capabilities. After reaching the final branched configuration, we remove a fraction of cells chosen at random and we allow



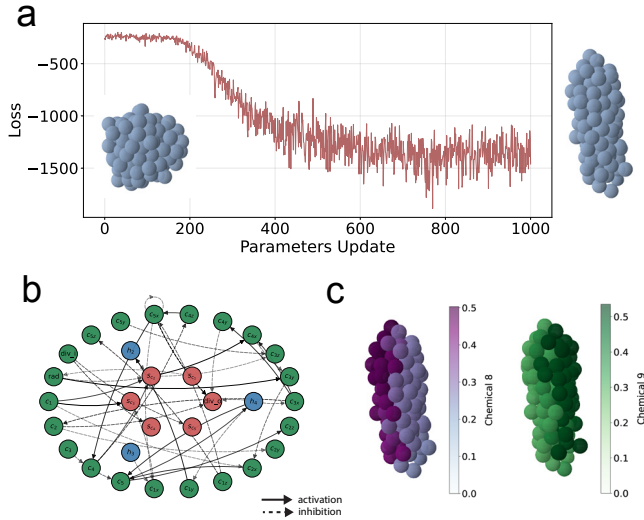


**FIG. 3. Elongation.** Maximization of the squared sum of the  $z$ -coordinates of cells, resulting in vertical elongation in the optimized cluster. (a) Loss curve for one successful optimization run. On the left the final configuration of a simulation with randomly initialized parameters, on the right the final state after learning. (b) Visualization of the optimized and pruned gene network, displaying activation and inhibition interactions that regulate cell behavior during elongation. (c) Two examples of emerging chemical gradients that are used to guide growth.

the cluster grow back to its original size. As shown in Fig 4d, eliminating up to 60% of cells still results in the regeneration of a branched structure. Even more interestingly, it appears that randomly removing cell actually promotes error-correction in the regrowth, reaching even slightly better performances in the training loss.

### MECHANICAL CONTROL OF CELL PROLIFERATION

Mechanical signaling has long been recognized as an important component of morphogenesis. In individual cells, mechanosensation influences gene expression through several identified biochemical pathways that can transduce forces [36]. On a tissue-level scale, mechanical signals can communicate local instructions to build a global shape [36–39]. In tissues, mechanical interactions can act on larger length scales than biochemical signals due to the propagation of tension through connected cells [39]. The buildup of local mechanical stress, additionally, can influence global growth of a developing structure. As an example, mechanical feedback has been posited as a mechanism for growth arrest in the wing imaginal disc of *Drosophila* [40, 41]. Here, we explore these ideas by optimizing over a model inspired by Hufnagel et al. to learn mechanisms that couple mechanics to growth.

In our model, a radial growth factor gradient scales a

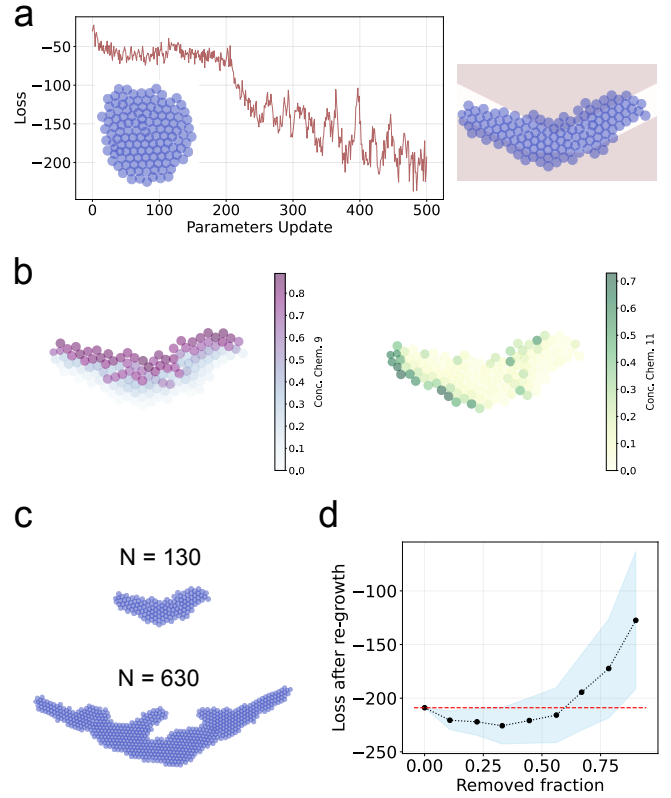


**FIG. 4. Branching.** Optimizing growth in a V-shaped reward landscape results in a learned branched structure of the final cluster. (a) Loss curve for one successful optimization run. On the left, the final configuration of a simulation with randomly initialized parameters. On the right, the final state after learning with a visualization of the reward mask (red areas are associated to penalties, white ones with rewards). (b) Two examples of emerging chemical gradients that are used to guide growth. (c) Final optimized state after 129 cell divisions, the same number used for the training (top) and with 500 extra cell divisions. Note the spontaneous branching on the main arms. (d) Loss of the final state after removal, at random, of a fraction of cells. The red dashed line is the loss associated to the final simulation state before cell removals.

division propensity calculated by gene networks in each cell, such that cells closer to the origin have a higher probability of division than cells at the edges (Fig. 5a). The growth factor gradient follows a power law and is fixed with respect to the simulation. We run the simulation for 200 cell division steps starting from one cell, with each cell modulating its secretion of two morphogens and its division propensity. We seek local growth rules that achieve homogeneous growth (homogeneous division propensities) throughout the cluster despite the nonuniform effect of the growth factor. The gene network that calculates the propensity of division does not see the growth factor as an input; therefore, cells have to infer this information by sensing stress or communicating through morphogens. The learned gene network can sense morphogen concentrations, morphogen gradients,

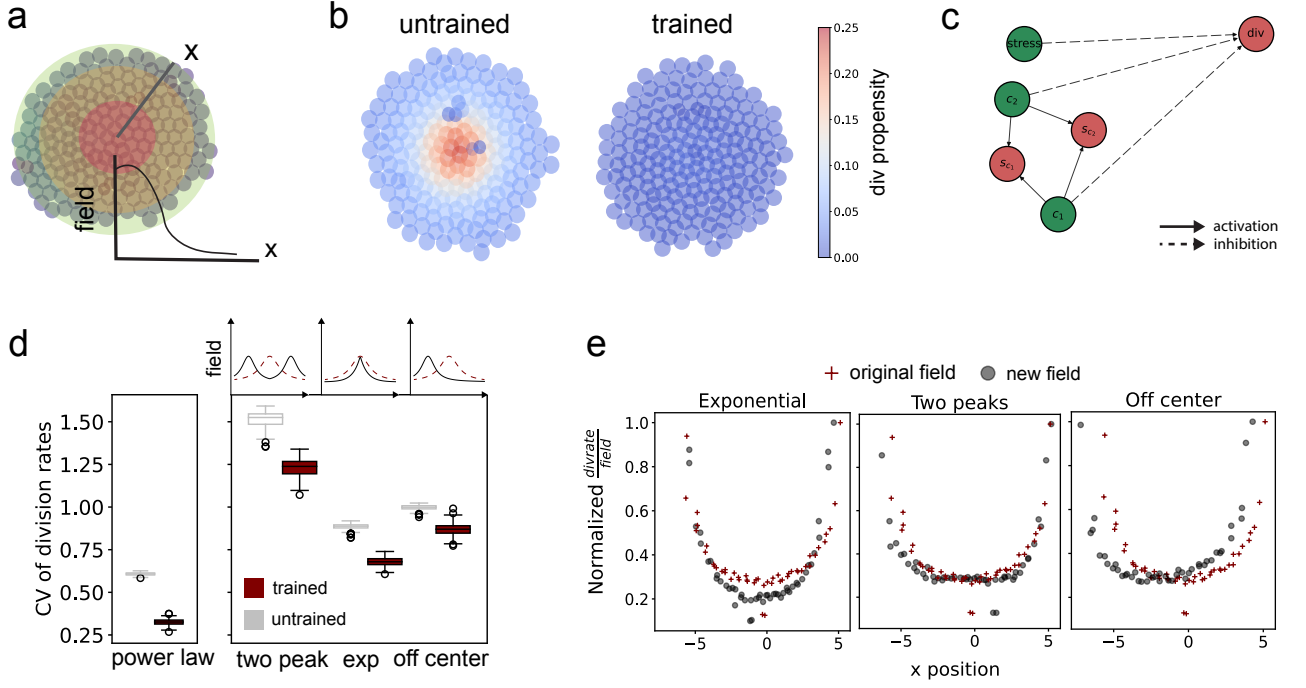


FIG. 5. **Mechanical Mechanisms for Homogeneous Growth.** (a) Schematic of setup of optimization problem for learning uniform growth and definition of loss function. (b) Visualization of the final configuration of the cluster from an optimized and unoptimized simulation. The unoptimized simulation does not regulate division propensities based on local inputs and thus, growth reflects the growth factor gradient. Cells are colored by the division propensity. (c) Visualization of trained gene network. (d) Gene network learned with a power law morphogen field readily works on three other kinds of morphogen fields: an exponential field, a field with two peaks instead of one, and a field with an off center peak. Losses are shown for each field type, averaged over 100 simulations. (e) Division rate divided by the morphogen field concentration is plotted for each kind of simulation from (d). This shows how cells regulate division probabilities without the influence of the field; results show that the way cells regulate division adapts to the kind of field due to the learned stress-based mechanism.

and stress as cellular inputs. We optimize couplings between genes that sense these inputs, four internal genes, and three output genes that modulate secretion rates of the two morphogens as well as the division propensity. The optimization minimizes the coefficient of variation of division propensities at the end of the simulation:

$$\mathcal{L} = CV[\mathbf{d}(T)] = \frac{\sigma[\mathbf{d}(T)]}{\mu[\mathbf{d}(T)]}$$

where  $\mathbf{d}(T)$  are the division propensities at final time  $T$ .

Simulations run using the optimized model show a clear separation between the final costs of simulations run using untrained versus trained parameters (Supp Fig. S4b). Visualization of simulations confirms that trained parameters resulted in homogeneous growth (Fig. 5b). The learned gene circuit utilized both chemical and mechanical information to modulate division propensity (Fig. 5c, Supp Fig. S4d). To probe the robustness of the learned mechanism, we apply the trained gene circuit to simulations with other types of growth factor gradients: (a) an exponentially decaying growth factor gradient, (b) a gradient with two symmetric peaks, and (c) a gradient

with a single asymmetric peak. Although we did not show any of these morphogen patterns during training, the gene circuit optimized on the power law gradient is still able to homogenize growth for the other types of gradients (Fig. 5d). Furthermore, the outputs of the gene network seem to track the shape of the fields, as well as patterns of stress accumulation (Fig. 5e, Supp Fig. S4c), consistently with a mechanical feedback mechanism. This is reminiscent of the mechanism proposed by Hufnagel et al., where nonuniform growth leads to a buildup of mechanical stress at the center of the cluster, providing a feedback signal that cells can use to regulate their growth rates.

## CHEMICAL REGULATION OF TISSUE HOMEOSTASIS

Maintaining stable ratios of various cell populations in tissue is important for proper functioning, and disruption of this can lead to disease [42]. To stably maintain homeostasis, the underlying cellular circuitry must prevent runaway growth for either cell type. Cells communi-

cate via growth factors, and cell circuits that receive and send growth factors maintain tissue homeostasis, sometimes regenerating after perturbations. For example, co-cultures of macrophages and fibroblasts can reach stable ratios, even if initially plated with ratios that differ 100-fold [43]. Here, we aim at learning chemical mechanisms that can maintain a 50/50 ratio of two different cell types in a growing cell cluster.

In our model, two cell types are instantiated, each secreting one of two different chemicals. The simulation is seeded with an imbalanced initial state of  $N_{init} = 20$  total cells and  $n_r = 4$  red cells, and uniform division propensities. After 100 cell divisions, this results in a final cluster that preserves the initial imbalance (Fig 6a left). Gene interaction couplings are then optimized to minimize the number difference between the two cell types during growth (Fig 6a right). The loss at time  $t$  takes the form:

$$\mathcal{L}_t = |n_r(t) - n_b(t)|$$

where  $n_r$  and  $n_b$  are the number of red and blue cells respectively, with  $n_r + n_b = N$  being the total number of cells at time  $t$ .

Cells can take division decisions only based on local communication of chemicals, and therefore they must infer information about population differences from chemical interactions. The optimization procedure successfully learns mechanisms that decrease the initial imbalance – such as the one depicted in Fig. 6b – resulting in equal proportions of cell types. Fig. 6c shows instead the chemical landscape associated with the learned final state, where one can observe the chemicals being associated with the two different cell types. Remarkably, the learned gene regulation displays robustness and generalization properties that were not explicitly optimized for. Fixing the initial imbalance to the one used during training ( $n_r/N = .2$ ), even though the training simulations only go through 100 cell divisions, the learned regulation maintains homeostasis also for simulations that run for much longer with no sign of efficiency degradation (Fig. 6d). If we instead fix the number of cell divisions to 100 and change the initial state imbalance, we observe in Fig. 6e that homeostasis is reasonably maintained for up to almost twice the initial imbalance. After this threshold the circuit starts to over-compensate, and loses its advantage over completely random cell divisions. We can also learn simpler mechanisms by allowing each cell type to implement and learn its own network own genetic program. This results in a smaller number of solutions with very sparse connectivity, that are easier to interpret (see Supp. Fig. S2).

## DISCUSSION

Our results demonstrate the power of gradient-based optimization methods in discovering mechanisms within

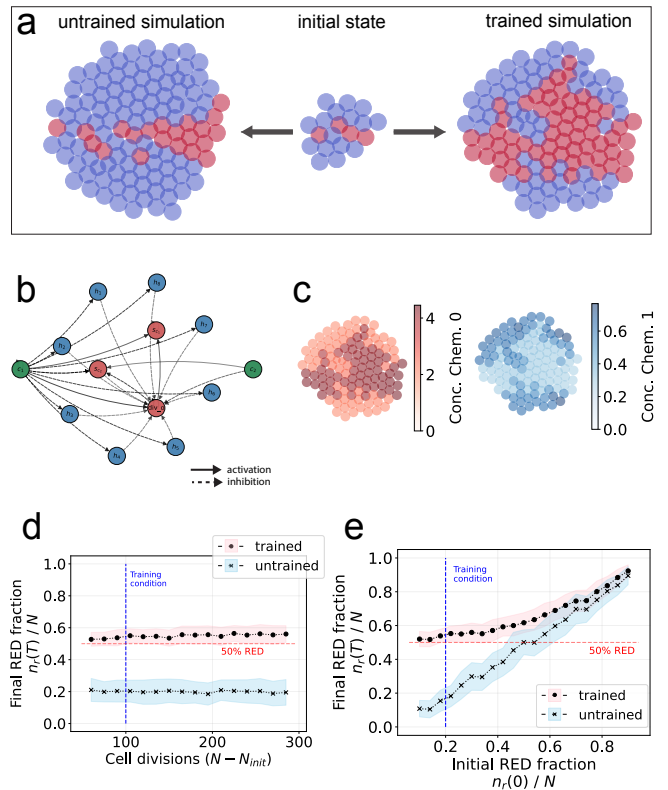


**FIG. 6. Chemical Regulation of Homeostasis.** (a) An initially imbalanced state (in the middle) grows into an equally unbalanced final state with untrained network parameters (left) and into a balanced state with learned parameters (right) (b) Visualization of the learned gene network. (c) Visualization of the chemical concentrations at the final state of the optimized simulation. (d) Average over 100 realizations of final proportion of red cells at the end of simulations of increasing lengths. (e) Average over 100 realizations of final proportion of red cells at the end of simulations with increasing proportions of red cells in the starting state. In both plots the shaded area corresponds to average plus or minus one standard deviation. (f) Visualization of learned gene networks when each cell type can learn its own network.

the space of physical, cell-based models for collective behavior. By taking gradients through a physical model of cells interacting written using differentiable code, we were able to learn decision-making programs within individual cells to orchestrate growth into target shapes or with target properties. Additionally, we were able to overcome challenges associated with differentiating through the discrete nature of cell division events and non-differentiable loss functions through reinforcement learning based approaches. The mechanisms that were learned took the form of gene regulatory networks, which readily offer a biological interpretation. The learned mechanisms were local in nature; cells did not have access to global positional information and had to instead infer it by sensing chemicals and mechanics and communicating with nearby cells through these physical

channels.

Although the gene networks optimized here are too large to instantiate experimentally, they could be distilled to find minimal networks or constrained to incorporate prior biological knowledge. Furthermore, the soft sphere model we have presented here is simply one of the possible choices. The physical details can be modified to optimize over an appropriate forward model with the same methods we demonstrated in this work. Questions about minimal mechanisms, robustness to variation and perturbations, number of unique solutions or growth principles could also be framed and investigated within the same setting.

Our results are a promising first step towards inferring mechanisms in existing multicellular systems or learning how to program them for desired behaviors. In particular, morphogenetic mechanisms frequently utilize local feedback to coordinate intricate forms, often through chemical or mechanical signals. Examples include a myriad of developmental systems, from the development of the wing imaginal disc in *Drosophila* to the periodic segmentation of blocks in somitogenesis. The development of robust and useful organoid systems also requires an understanding of spatiotemporal chemical and physical cues needed to guide the growth of stem cells. Physical models could be optimized to reproduce experimental data from time-lapse imaging of such developmental systems to gain insights into individual decision making functions that recapitulate complex behaviors. Gene expression datasets could be incorporated to bridge the gap between known and unknown information in biological systems. Our work opens up a multitude of avenues for further explorations of the landscape of growth programs for desired emergent behaviors in living systems.

## MATERIALS AND METHODS

Fully differentiable, hardware-accelerated simulations were coded using the JAX python library [24] and other libraries in the JAX ecosystem. In particular, JAX-MD [26] was used to perform molecular dynamics simulations for cell mechanics and Equinox [25] as the simulation backbone.

We proceed to give a very succinct overview of the main components of our model. A full mathematical account of simulation and optimization details is given in the *Supplementary Information*.

### Cell division and growth

Each cell  $i$  is endowed with a *division propensity*  $d_i$  calculated by the internal gene network. One cell divides at each time step, with probability:

$$P(i \text{ divides}) = \frac{d_i}{\sum_i d_i}$$

The division substitutes one mature cell with two new-born cells with half the volume. The angular orientation of the division plan is chosen uniformly at random.

Cells' radii  $R_i$  grow linearly in time up to a maximum radius  $R_{max}$ :

$$R_i(t + \Delta t) = \min(R_i(t) + \Delta R, R_{max})$$

### Mechanical interactions

Cells are modeled as adhesive soft spheres. Interactions are defined by the Morse energy potential:

$$V_{ij}(r) = \epsilon_{ij} \left[ 1 - e^{-\alpha_{ij}(r_{ij} - \sigma_{ij})} \right]^2 - \epsilon_{ij}$$

where  $\epsilon_{ij}$  is the well depth for the potential between particle  $i$  and  $j$ ,  $\alpha_{ij}$  is the range of interaction,  $\sigma_{ij}$  is the sum of radii of particles  $i$  and  $j$ , and  $r_{ij}$  is the distance between the two particles.

### Diffusion

We assume that chemicals diffuse freely in the environment and are taken up by cells at a constant rate. It is also assumed that diffusion is much faster than all other processes and can be therefore be considered at steady state. For any one chemical  $k$ :

$$\frac{\partial c_k}{\partial t} = D_k \nabla^2 c_k - K_k c_k + S_k = 0$$

The equation is discretized and solved on the lattice formed by the cells' centers with the graph Laplacian technique.

### Genetic regulatory interactions

We model internal cell decision functions with a simple ODE model of gene regulation inspired by Hiscock [22]:

$$\frac{dg_i}{dt} = \phi(\sum_j W_{ij} g_j) + I_i - k_i g_i$$

Considering the  $i$ -th gene,  $g_i$  is the expression level,  $W_{ij}$  is the regulatory influence of gene  $j$  on  $i$ ,  $k_i$  is the degradation rate, and  $I_i$  is a forcing signal coming from one of the sensed cell inputs.  $\phi$  is a sigmoid function that ensures positive transcription rates saturating at high input levels.

## Gradient calculation

The gradient of simulations in Fig. 2 is calculated with standard automatic differentiation. The gradients of all the other simulations involve dealing with cell division events. Following REINFORCE [27], we can estimate the gradient of the expected loss for a single simulation:

$$\nabla_{\theta} \mathcal{L}(\theta) \approx \sum_{t=0}^{T-1} L_t \nabla_{\theta} \log \pi_{\theta}(a_t | s_t)$$

where  $L_t$  is the discounted future loss,  $\theta$  represents the trainable gene network parameters and  $\pi$  is the probability of the division event parametrized by  $\theta$ .

## ACKNOWLEDGMENTS

This work is dedicated to the memory of Alma Dal Co.

We thank for insightful discussions: the members of the Brenner Group, the members of the former Dal Co group, Boris Shraiman and Dillon Cislo. R.D. thanks Hervé Turlier for helpful discussions. This work was supported by the Office of Naval Research through grant numbers ONR N00014-17-1-3029, ONR N00014-23-1-2654 and the NSF AI Institute of Dynamic Systems (2112085).

## DATA AVAILABILITY

The custom library written to conduct this study is available at <https://github.com/fmottes/jax-morph/>, along with tutorial notebooks.

- 
- [1] M. Rubenstein, A. Cornejo, and R. Nagpal, Programmable self-assembly in a thousand-robot swarm, *Science* **345**, 795 (2014).
  - [2] C. Collinet and T. Lecuit, Programmed and self-organized flow of information during morphogenesis, *Nature Reviews Molecular Cell Biology* **22**, 245 (2021).
  - [3] J. Davies, Using synthetic biology to explore principles of development, *Development (Cambridge, England)* **144**, 1146 (2017).
  - [4] J. J. Velazquez, E. Su, P. Cahan, and M. R. Ebrahimkhani, Programming Morphogenesis through Systems and Synthetic Biology, *Trends in biotechnology* **36**, 415 (2018).
  - [5] Y. Ma, M. W. Budde, M. N. Mayalu, J. Zhu, A. C. Lu, R. M. Murray, and M. B. Elowitz, Synthetic mammalian signaling circuits for robust cell population control, *Cell* **185**, 967 (2022).
  - [6] S. Toda, W. L. McKeithan, T. J. Hakkinen, P. Lopez, O. D. Klein, and W. A. Lim, Engineering synthetic morphogen systems that can program multicellular patterning, *Science (New York, N.Y.)* **370**, 327 (2020).
  - [7] M. A. Lancaster, N. S. Corsini, S. Wolfinger, E. H. Gustafson, A. Phillips, T. R. Burkard, T. Otani, F. J. Livesey, and J. A. Knoblich, Guided self-organization and cortical plate formation in human brain organoids, *Nature biotechnology* **35**, 659 (2017).
  - [8] A. Lewis, R. Keshara, Y. H. Kim, and A. Grapin-Botton, Self-organization of organoids from endoderm-derived cells, *Journal of Molecular Medicine* **99**, 449 (2021).
  - [9] J. A. Brassard and M. P. Lutolf, Engineering Stem Cell Self-organization to Build Better Organoids, *Cell Stem Cell* **24**, 860 (2019).
  - [10] M. M. Stijns, V. L. LaPointe, and C. A. van Blitterswijk, Building Complex Life Through Self-Organization, *Tissue Engineering. Part A* **25**, 1341 (2019).
  - [11] S. Werner, H. T.-K. Vu, and J. C. Rink, Self-organization in development, regeneration and organoids, *Current Opinion in Cell Biology Cell Architecture*, **44**, 102 (2017).
  - [12] M. Hofer and M. P. Lutolf, Engineering organoids, *Nature Reviews Materials* **6**, 402 (2021).
  - [13] J. M. Osborne, A. G. Fletcher, J. M. Pitt-Francis, P. K. Maini, and D. J. Gavaghan, Comparing individual-based approaches to modelling the self-organization of multicellular tissues, *PLoS Computational Biology* **13**, e1005387 (2017).
  - [14] S. Runser, R. Vetter, and D. Iber, Simucell3d: three-dimensional simulation of tissue mechanics with cell polarization, *Nature Computational Science* **4**, 299 (2024).
  - [15] R. Anil, A. M. Dai, O. Firat, M. Johnson, D. Lepikhin, A. Passos, S. Shakeri, E. Taropa, P. Bailey, Z. Chen, *et al.*, Palm 2 technical report, arXiv preprint arXiv:2305.10403 (2023).
  - [16] T. Brown, B. Mann, N. Ryder, M. Subbiah, J. D. Kaplan, P. Dhariwal, A. Neelakantan, P. Shyam, G. Sastry, A. Askell, *et al.*, Language models are few-shot learners, *Advances in neural information processing systems* **33**, 1877 (2020).
  - [17] C. P. Goodrich, E. M. King, S. S. Schoenholz, E. D. Cubuk, and M. P. Brenner, Designing self-assembling kinetics with differentiable statistical physics models, *Proceedings of the National Academy of Sciences* **118**, e2024083118 (2021).
  - [18] Y. Bar-Sinai, S. Hoyer, J. Hickey, and M. P. Brenner, Learning data-driven discretizations for partial differential equations, *Proceedings of the National Academy of Sciences* **116**, 15344 (2019).
  - [19] M. C. Engel, J. A. Smith, and M. P. Brenner, Optimal control of nonequilibrium systems through automatic differentiation, *Physical Review X* **13**, 041032 (2023).
  - [20] R. A. Vargas-Hernández, R. T. Q. Chen, K. A. Jung, and P. Brumer, Fully differentiable optimization protocols for non-equilibrium steady states, *New Journal of Physics* **23**, 123006 (2021).

- [21] A. Mordvintsev, E. Randazzo, E. Niklasson, and M. Levin, Growing Neural Cellular Automata, *Distill* **5**, e23 (2020).
- [22] T. W. Hiscock, Adapting machine-learning algorithms to design gene circuits, *BMC Bioinformatics* **20**, 214 (2019).
- [23] H. Koyama, H. Okumura, A. M. Ito, K. Nakamura, T. Otani, K. Kato, and T. Fujimori, Effective mechanical potential of cell–cell interaction explains three-dimensional morphologies during early embryogenesis, *PLOS Computational Biology* **19**, e1011306 (2023), publisher: Public Library of Science.
- [24] J. Bradbury, R. Frostig, P. Hawkins, M. J. Johnson, C. Leary, D. Maclaurin, G. Necula, A. Paszke, J. VanderPlas, S. Wanderman-Milne, and Q. Zhang, JAX: composable transformations of Python+NumPy programs (2018).
- [25] P. Kidger and C. Garcia, Equinox: neural networks in JAX via callable PyTrees and filtered transformations, *Differentiable Programming workshop at Neural Information Processing Systems 2021* (2021).
- [26] S. S. Schoenholz and E. D. Cubuk, Jax m.d. a framework for differentiable physics, in *Advances in Neural Information Processing Systems*, Vol. 33 (Curran Associates, Inc., 2020).
- [27] R. S. Sutton and A. G. Barto, *Reinforcement Learning: An Introduction*, 2nd ed. (The MIT Press, 2018).
- [28] <https://github.com/fmottes/jax-morph/tree/eqx/tutorials> (2024), accessed: 2024-07-06.
- [29] D. P. Kingma and J. Ba, Adam: A Method for Stochastic Optimization (2017), arXiv:1412.6980 [cs].
- [30] M. S. Steinberg, Does differential adhesion govern self-assembly processes in histogenesis? Equilibrium configurations and the emergence of a hierarchy among populations of embryonic cells, *Journal of Experimental Zoology* **173**, 395 (1970), eprint: <https://onlinelibrary.wiley.com/doi/pdf/10.1002/jez.1401730406>.
- [31] T. Y.-C. Tsai, M. Sikora, P. Xia, T. Colak-Champollion, H. Knaut, C.-P. Heisenberg, and S. G. Megason, An adhesion code ensures robust pattern formation during tissue morphogenesis, *Science* **370**, 113 (2020), publisher: American Association for the Advancement of Science.
- [32] M. Bao, J. Cornwall-Scoones, E. Sanchez-Vasquez, A. L. Cox, D.-Y. Chen, J. De Jonghe, S. Shadkhoo, F. Hollfelder, M. Thomson, D. M. Glover, and M. Zernicka-Goetz, Stem cell-derived synthetic embryos self-assemble by exploiting cadherin codes and cortical tension, *Nature Cell Biology* **24**, 1341 (2022), publisher: Nature Publishing Group.
- [33] Y. Guo, M. Nitzan, and M. P. Brenner, Programming cell growth into different cluster shapes using diffusible signals, *PLOS Computational Biology* **17**, e1009576 (2021).
- [34] S. Darras, J. H. Fritzenwanker, K. R. Uhlinger, E. Farrelly, A. M. Pani, I. A. Hurley, R. P. Norris, M. Osovitz, M. Terasaki, M. Wu, J. Aronowicz, M. Kirschner, J. C. Gerhart, and C. J. Lowe, Anteroposterior axis patterning by early canonical wnt signaling during hemichordate development, *PLoS Biology* **16**, e2003698 (2018).
- [35] D. Iber and D. Menshykau, The control of branching morphogenesis, *Open Biology* **3**, 130088 (2013).
- [36] P. Agarwal and R. Zaidel-Bar, Mechanosensing in embryogenesis, *Current Opinion in Cell Biology Cell Architecture*, **68**, 1 (2021).
- [37] K. D. Irvine and B. I. Shraiman, Mechanical control of growth: ideas, facts and challenges, *Development* **144**, 4238 (2017).
- [38] D.-C. Trinh, J. Alonso-Serra, M. Asaoka, L. Colin, M. Cortes, A. Malivert, S. Takatani, F. Zhao, J. Traas, C. Trehin, and O. Hamant, How Mechanical Forces Shape Plant Organs, *Current biology: CB* **31**, R143 (2021).
- [39] L. LeGoff, H. Rouault, and T. Lecuit, A global pattern of mechanical stress polarizes cell divisions and cell shape in the growing *Drosophila* wing disc, *Development* **140**, 4051 (2013).
- [40] B. I. Shraiman, Mechanical feedback as a possible regulator of tissue growth, *Proceedings of the National Academy of Sciences* **102**, 3318 (2005), publisher: Proceedings of the National Academy of Sciences.
- [41] L. Hufnagel, A. A. Teleman, H. Rouault, S. M. Cohen, and B. I. Shraiman, On the mechanism of wing size determination in fly development, *Proceedings of the National Academy of Sciences* **104**, 3835 (2007), publisher: Proceedings of the National Academy of Sciences.
- [42] J. Hicks-Berthet, B. Ning, A. Federico, A. Tilston-Lunel, A. Matschulat, X. Ai, M. E. Lenburg, J. Beane, S. Monti, and X. Varelas, Yap/taz inhibit goblet cell fate to maintain lung epithelial homeostasis, *Cell Reports* **36**, 109347 (2021).
- [43] X. Zhou, R. A. Franklin, M. Adler, J. B. Jacox, W. Bailis, J. A. Shyer, R. A. Flavell, A. Mayo, U. Alon, and R. Medzhitov, Circuit Design Features of a Stable Two-Cell System, *Cell* **172**, 744 (2018), publisher: Elsevier.



# SUPPLEMENTARY INFORMATION

## Engineering morphogenesis of cell clusters with differentiable programming

Ramya Deshpande\*, Francesco Mottes\*, Ariana-Dalia Vlad, Michael Brenner and Alma Dal Co

### CONTENTS

I. Forward Simulation	2
Cell Growth	2
Mechanical Interactions	2
Cell Division	2
Diffusion	3
Chemical Gradients	4
Mechanical Stress	4
Gene Networks	4
II. The REINFORCE Optimization Algorithm	4
A. Underlying Theory	4
Markov Decision Processes	4
Policy Gradients Theorem	5
Monte Carlo Estimation	6
Parameters Update Rule	6
Baseline for Variance Reduction	6
B. Optimization of Cell Divisions	6
III. Experiment Details	7
Chemical Regulation of Cellular Adhesion	7
Elongation	9
Branching	9
Chemical Homeostasis	9
Mechanical Control of Cell Proliferation	12
IV. Scaling of Optimization Performance with Model Complexity	14

## I. FORWARD SIMULATION

We run simulations using JAX-MD, a molecular dynamics engine built using the automatic differentiation framework JAX. Cells are particles instantiated in "free" space, with a set of properties represented by a `CellState` datatype; this object contains the position of particles, their radii, division propensities, chemical concentrations at the center of each cell and any additional state information appropriate for a simulation (for example: stress, finite difference gradients of the chemical concentrations, etc.). At the start of the simulation, arrays of size  $(T, n + T, \text{Dim})$  are instantiated for each property in `CellState`, where  $T$  is the number of timesteps,  $n$  is the initial number of cells, and  $\text{Dim}$  is the dimension of the cell property (2D or 3D). Each simulation timestep consists of one cell division, so the final configuration will contain  $N = n + T$  cells.

To create an initial state with  $n$  cells, we place a cell at the origin, and run  $n - 1$  iterations of cell division, cell growth, and mechanical relaxation to generate a cluster of the desired initial size. All division propensities are equal in the initial state, so each cell is chosen to divide with equal probability, generating a radially symmetric cluster. The actual simulation can be customized to contain any subset or combination of the steps detailed below; the specifics of the simulation used for each instantiation in the main text is detailed in the *Experimental Details* section. The code used for the simulations can be found in the following GitHub repository: <https://github.com/fmottes/jax-morph>.

### Cell Growth

All cell radii grow constantly in time, up to a specified maximum radius  $R_{\max}$ :

$$R_i(t + \Delta t) = \min(R_i(t) + \Delta R, R_{\max})$$

This operation can also be made differentiable if necessary, by means of a suitable smoothing function in place of the hard *min* operation.

### Mechanical Interactions

Cells mechanically interact with one another via a pairwise Morse potential. The potential has a minimum at a distance defined by the sum of the two interacting cells' radii. It is very repulsive at shorter distances (*volume-exclusion interactions*) and slightly attractive at longer distances (*cell-cell adhesion*). The range of attraction, the strength of the exclusion and the stiffness of the interaction can be modified by changing the potential parameters.

Relaxation is performed by gradient descent energy minimization of the Morse potential for a fixed number of steps (except in the case where we learn cell adhesion). The pairwise potential is defined by the following expression:

$$V_{ij}(r) = \epsilon_{ij} \left[ 1 - e^{-\alpha_{ij}(r_{ij} - \sigma_{ij})} \right]^2 - \epsilon_{ij}$$

where  $\epsilon_{ij}$  is the well depth for the potential between particle  $i$  and  $j$ ,  $\alpha_{ij}$  is the range of interaction,  $\sigma_{ij}$  is the sum of radii of particles  $i$  and  $j$ , and  $r_{ij}$  is the distance between the two particles. In most simulations, we assume for simplicity that  $\alpha_{ij} = \alpha$  and  $\epsilon_{ij} = \epsilon$ . This need not be the case in general. In particular, in the example where we learn the regulation of cell-to-cell adhesion, the values of  $\epsilon_{ij}$  are determined by the cells' internal regulatory mechanisms.

### Cell Division

Each cell  $i$  is endowed with a *division propensity*  $d_i$  calculated by the internal gene network and stored in the `CellState`. One cell divides at each time step, with probability:

$$P(i \text{ divides}) = \frac{d_i}{\sum_j d_j}$$

A cell  $i$  is first randomly chosen to divide with these probabilities. A random direction is then selected as  $\theta \in [0, 2\pi]$ . The positions of the daughter cells are calculated as:

$$\bar{r}_{1,x} = \bar{r}_{0,x} + R_{\text{birth}} \cos(\theta), \bar{r}_{1,y} = \bar{r}_{0,y} + R_{\text{birth}} \sin(\theta) \quad (1)$$

$$\bar{r}_{2,x} = \bar{r}_{0,x} - R_{\text{birth}} \cos(\theta), \bar{r}_{2,y} = \bar{r}_{0,y} - R_{\text{birth}} \sin(\theta) \quad (2)$$

where  $(\bar{r}_{1,x}, \bar{r}_{1,y})$  and  $(\bar{r}_{2,x}, \bar{r}_{2,y})$  are the positions of the daughter cells,  $(\bar{r}_{0,x}, \bar{r}_{0,y})$  is the position of the mother cell and  $R_{\text{birth}}$  is fixed as the radius of newly born cells. Each daughter cell inherits all other properties of its mother cell.

### Diffusion

We assume that chemicals diffuse freely in the environment and are taken up by cells at a constant rate. It is also assumed that diffusion is much faster than all other processes and can be therefore be considered at steady state. Concentrations of a chemical  $k$  (in arbitrary units) at each cell site are determined by the following equation:

$$\frac{\partial c_k}{\partial t} = D_k \nabla^2 c_k - K_k c_k + S_k = 0$$

The equation is discretized and solved on the lattice formed by the cells' centers with the graph Laplacian technique. The PDE above is first reformulated by substituting the diffusion operator with the discrete graph Laplacian  $L$ . This results in a linear system of ODEs for each chemical, describing the concentration of a chemical on each lattice site. The equation is then solved for the steady state concentrations  $\{\mathbf{c}_k\}$ :

$$\frac{\partial \mathbf{c}_k}{\partial t} = D_k L \mathbf{c}_k - K_k \mathbf{c}_k + \mathbf{S}_k = 0$$

$D_k$  is the diffusion coefficient of chemical  $k$  and  $K_k$  is the uptake rate for chemical  $k$ , the same for every cell for simplicity.  $\mathbf{S}_k$  is an  $N \times 1$  vector of secretion rates of chemical  $k$  by every cell, calculated by the gene networks.  $\mathbf{c}_k$  is an  $N \times 1$  vector containing the concentration of chemical  $k$  at all cell sites. The discrete graph Laplacian operator is constructed as:

$$L = \text{deg}(A) - A$$

where  $A$  is the adjacency matrix that describes the connections between the discrete spatial sites.  $\text{deg}(A)$  is a matrix that has the sum of  $A$ 's rows (that is, the node degrees) as diagonal elements and is zero everywhere else. For all cells  $i$ :

$$\{\text{deg}(A)\}_{ii} = \sum_{j=0}^N A_{ij}$$

Apart from the branching and homogeneous growth examples, we construct the graph Laplacian to simulate diffusion in a closed system with reflecting boundary conditions. In this case the adjacency matrix  $A$  is calculated as the inverse of the pairwise distance between every pair of cells:

$$A_{ij} = \frac{1}{\text{dist}(i, j)} = \frac{1}{\|\bar{r}_i - \bar{r}_j\|}$$

In order to simulate permeable boundaries without the additional burden of having a higher resolution lattice only for chemical diffusion, we adopt an approximate approach. We now construct the adjacency matrix by connecting cells that are nearest neighbors with an edge of weight 1 (that is approximately their distance) and zero otherwise:

$$A_{ij} = \begin{cases} 1 & \text{if } \text{dist}(i, j) \leq R_i + R_j \\ 0, & \text{otherwise} \end{cases}$$

We then heuristically detect the nodes that are on the boundaries of the cluster by looking at the number of nodes they are connected to. We connect all of these boundary nodes to a ghost sink node that receives and dissipates chemicals, to simulate the effect of chemicals lost in the medium surrounding the cluster. In practice, this is done by adding, in the degree matrix, an extra unit of degree to the nodes on the boundary.

### Chemical Gradients

Multicellular collectives can infer weak concentration gradients across the collective through individual cells measuring differences in chemical concentrations across their diameters. To achieve such an estimate of the spatial gradient of chemical  $k$  sensed by cell  $j$ , a unit vector pointing to each nearest neighbor  $i$  of cell  $j$  is scaled by the concentration of chemical  $k$  in those cells, and the contributions from all neighbors are summed up:

$$\nabla c_k(\bar{r}_j) \approx \sum_{i \in nn(j)} c_k(\bar{r}_i) \frac{\bar{r}_i - \bar{r}_j}{\|\bar{r}_i - \bar{r}_j\|} \quad (3)$$

Here,  $\bar{r}_i$  is the position of cell  $i$ , and  $c_k(\bar{r}_i)$  is the concentration of chemical  $k$  at position  $\bar{r}_i$ .

### Mechanical Stress

As a proxy for the mechanical stress exerted by cell  $i$  on cell  $j$  in our 2D environment, the component-wise force on  $i$  by  $j$ ,  $(F_{ij,x}, F_{ij,y})$ , is multiplied by the component-wise unit vector pointing from  $j$  to  $i$ ,  $(\bar{r}_{j,x} - \bar{r}_{i,x}, \bar{r}_{j,y} - \bar{r}_{i,y})$ ; this is summed over the components. For cell  $i$  we compute:

$$\sigma_i = \sum_j \left[ F_{ij,x} \cdot \frac{\bar{r}_{j,x} - \bar{r}_{i,x}}{|\bar{r}_{j,x} - \bar{r}_{i,x}|} + F_{ij,y} \cdot \frac{\bar{r}_{j,y} - \bar{r}_{i,y}}{|\bar{r}_{j,y} - \bar{r}_{i,y}|} \right]$$

This formulation allows for differentiation between compressive and tensile forces.

### Gene Networks

Methods presented in Hiscock et al. are adapted to model  $N$  genes that can interact with each other, with the sign of the interaction term determining whether it is an activating or inhibitory coupling. Weights of the gene networks are shared by all cells, in the same spirit in which actual cells share the same genetic material. Gene networks are specified by the following ODE model:

$$\frac{dg_i}{dt} = \phi(\sum_j W_{ij} g_j) + I_i - k_i g_i \quad (4)$$

Considering the  $i$ -th gene,  $g_i$  is the expression level,  $W_{ij}$  is the regulatory influence of gene  $j$  on  $i$ ,  $k_i$  is the degradation rate, and  $I_i$  is a forcing signal coming from one of the sensed cell inputs.  $\phi$  is a sigmoid function that ensures positive transcription rates saturating at high input levels. Local signals sensed by the cell (chemicals, stress, etc.) are fed as input signal to input nodes in the network (colored green in the diagrams in the main text). All other genes receive no external inputs. The last output gene's readout is the division propensity, and the last  $N_c$  genes readout the secretion rates of chemicals. In the case where cellular adhesion is chemically regulated, there are also output genes that readout cadherin concentrations.

## II. THE REINFORCE OPTIMIZATION ALGORITHM

### A. Underlying Theory

REINFORCE is a widely used reinforcement learning algorithm that allows to optimize the action policy directly, in a context where stochastic decisions must be taken. This is the algorithm we use for most of our optimizations, and below are the main steps in its derivation.

### Markov Decision Processes

We assume that our simulation follows a Markov Decision Process (MDP). That is, the probability of a trajectory  $\tau$  is the product of the probability of the initial state and the probabilities of each action and state transition along

the trajectory. Let  $\tau = (s_0, a_0, s_1, a_1, \dots, s_T, a_T)$  represent a trajectory, where  $s_t$  and  $a_t$  are the state and action (cell division) at time  $t$ , respectively. Assume  $\pi(a_t|s_t)$  is the policy (the division propensity calculated by the gene network),  $P(s_{t+1}|s_t, a_t)$  is the state transition probability, and  $P(s_0)$  is the initial state distribution. The probability of the trajectory  $\tau$  is given by:

$$P(\tau) = P(s_0) \prod_{t=0}^T \pi(a_t|s_t) P(s_{t+1}|s_t, a_t)$$

Where:

$P(s_0)$  is the probability of the initial state  $s_0$

$\pi(a_t|s_t)$  is the probability of taking action  $a_t$  given state  $s_t$

$P(s_{t+1}|s_t, a_t)$  is the probability of transitioning to state  $s_{t+1}$  given state  $s_t$  and action  $a_t$ .

### Policy Gradients Theorem

The goal is to maximize the expected return  $J(\theta)$ , where  $\theta$  are the parameters of the policy  $\pi_\theta(a|s)$ . The expected return is defined as:

$$J(\theta) = \mathbb{E}_{\pi_\theta} [G_t]$$

where  $G_t$  is the (possibly discounted) return starting from time step  $t$ . The expected gradient of the return with respect to the policy parameters  $\theta$  can be computed using the log-derivative trick, also known as the REINFORCE algorithm. The expected return  $J(\theta)$  is given by:

$$J(\theta) = \sum_{\tau} P(\tau) G(\tau)$$

The gradient of the expected return is:

$$\nabla_{\theta} J = \nabla_{\theta} \sum_{\tau} P(\tau) G(\tau) = \sum_{\tau} G(\tau) \nabla_{\theta} P(\tau)$$

Using the log-derivative trick,  $\nabla_{\theta} P(\tau)$  can be written as:

$$\nabla_{\theta} P(\tau) = P(\tau) \nabla_{\theta} \log P(\tau)$$

Thus, the expected gradient is:

$$\nabla_{\theta} J(\theta) = \sum_{\tau} P(\tau) G(\tau) \nabla_{\theta} \log P(\tau)$$

Using the definition of MDP given above, the gradient of the expected return with respect to  $\theta$  can be simplified to only include the policy  $\pi_\theta$ :

$$\nabla_{\theta} J(\theta) = \mathbb{E}_{\pi_\theta} [\nabla_{\theta} \log \pi_\theta(a|s) G_t]$$

### Monte Carlo Estimation

In practice, the expectation is estimated using Monte Carlo sampling. By sampling trajectories  $\tau = (s_0, a_0, r_0, s_1, a_1, r_1, \dots)$  from the policy  $\pi_\theta$ , the gradient can be approximated as:

$$\nabla_\theta J(\theta) \approx \frac{1}{N} \sum_{i=1}^N \sum_{t=0}^{T-1} \nabla_\theta \log \pi_\theta(a_t^i | s_t^i) G_t^i$$

where  $N$  is the number of sampled trajectories, and  $T$  is the length of each trajectory.

### Parameters Update Rule

The REINFORCE algorithm updates the policy parameters  $\theta$  by gradient ascent (if we are considering the case of maximizing total rewards):

$$\theta \leftarrow \theta + \eta \nabla_\theta J(\theta)$$

where  $\eta$  is the learning rate. In order to calculate the actual update, we substitute the Monte Carlo gradient estimate for the gradient derived above.

### Baseline for Variance Reduction

To reduce the variance of the gradient estimate, a baseline function  $b(s_t)$  is introduced, leading to the modified gradient:

$$\nabla_\theta J(\theta) = \mathbb{E}_{\pi_\theta} [\nabla_\theta \log \pi_\theta(a|s)(G_t - b(s_t))]$$

A common choice for the baseline is the state-value function  $V^\pi(s_t)$ , which represents the expected return from state  $s_t$ . Another common basic technique for variance reduction is to normalize the rewards after each batch of simulations, resulting in half of the actions being favored and half unfavored on average. We adopt the latter in this work.

## B. Optimization of Cell Divisions

In our simulations, we consider the policy to be the gene regulatory network inside each cell. Cells sense inputs from the environment and use them to decide how likely they should be to divide next. Notice that a loss applied naively at the end of the simulation — like for example a measure of distance from a given target — would produce undefined gradients. Stochastic operations (like sampling a cell for division) do not have a mathematically well-defined differentiation rule; therefore as soon as the back-propagation procedure encounters such operations, the whole gradient becomes ill-defined (or zero, in practice in the code). In order to overcome this obstacle, we resort to techniques like the one presented in the previous section.

Our simulation presents an additional complication with respect to the policy gradient case defined above. Cells influence the environment not only through their division decisions but also, mainly, through the modulation of chemical secretion. This creates a long feedback loop connecting secretions at one step to the chemical landscape at the next step, which in turn influences division decisions. As a consequence, the gradient of a loss applied to cell division events — like REINFORCE — must be propagated through the environment updates till the very beginning of the simulation. This makes automatic differentiation algorithms critical for this sort of optimization.

In all our optimizations, we use the Adam optimizer for gradient descent (hyperparameters are listed below). Reported losses, here and in the main text, are validation losses calculated on a batch of simulations different from the one used for updating the parameters.



### III. EXPERIMENT DETAILS

#### Chemical Regulation of Cellular Adhesion

The simulation is initialized with 60 cells and 3 cell types, and done in 3D. Cell positions and identities are randomly initialized. For the lattice and lobe structures, the cluster consists of equal numbers of each cell type (20 cells each); for optimizing a core-shell structure, the cluster consists of 10 blue cells, 20 yellow cells and 30 red cells. The simulation is run for 50 time steps, with 200 Brownian relaxation steps between each time step; the temperature is high to allow for sufficient rearrangement of the system without trapping. No cell division occurs. The simulation contains 64 internal genes, and each cell type can secrete 3 cell type specific morphogens. Diffusion occurs in a closed system.

*Cadherin.* The system contains  $N_{\text{ctype}} + 1$  cadherins, with each cell able to regulate concentrations of its cell type specific cadherin (*cad1*, *cad2*, etc.), as well as a heterotypic cadherin (*het*). The gene network takes as input sensed chemicals and regulates secretion rates of chemicals as well as the concentrations of cadherins. The well depth of the pairwise potential between cells is calculated as the sum of the concentration of homotypic cadherins (if they are the same cell type) or the sum of the concentration of heterotypic cadherins (if they are different cell types). This also ensures that the pairwise well depth matrix is always symmetric. The calculated well depth value is then scaled by a sigmoid to be between .8 and 3.8, ensuring a stable range of values are used for the Morse potential.

*Optimization.* Since there is no cell division in this simulation, we directly backpropagate through the simulation without using REINFORCE. To improve the quality of gradients when backpropagating through long simulations, we "discount" gradients in the backward pass by a discounting factor of 0.99 - this results in gradients from time steps closer to the end of the simulation providing a greater contribution to the optimization. Training is done over a batch of 4 simulations, and the validation loss is averaged over a batch of 64 simulations. Additionally, at each gradient descent step, we constrain the learned network by setting to zero all outgoing edges from output nodes. Three different loss functions are utilized. To learn a lobe-like arrangement, the following loss is used:

$$\frac{1}{N_t} \sum_t \sum_{\text{cell } i} \sum_{\text{cell } j} \begin{cases} \text{dist}(i, j), & \text{if type}(i) == \text{type}(j) \\ 0, & \text{otherwise} \end{cases}$$

This is the sum of pairwise distances between cells of the same type, averaged over all time steps of the simulation. Conversely, to attain a lattice-like structure, the sum of pairwise distances between unlike cell types is minimized:

$$\frac{1}{N_t} \sum_t \sum_{\text{cell } i} \sum_{\text{cell } j} \begin{cases} 0, & \text{if type}(i) == \text{type}(j) \\ \text{dist}(i, j), & \text{otherwise} \end{cases}$$

For the core-shell structure, the distance of cells from a predefined radius (based on the cell's type) with respect to the center of the core cells is minimized:

$$C = \frac{1}{N_1} \sum_{i \in \text{type 1 cells}} \bar{r}_i$$

$$\frac{1}{N_t} \sum_t \sum_{\text{cell } i} \begin{cases} (\text{dist}(i, C) - 1)^2, & \text{if type}(i) == 1 \\ (\text{dist}(i, C) - 2)^2, & \text{if type}(i) == 2 \\ (\text{dist}(i, C) - 3)^2, & \text{if type}(i) == 3 \end{cases}$$

Here,  $C$  is the average position of the core cells,  $N_1$  is the number of core cells,  $\text{type}(i)$  is the cell type of cell  $i$ , and  $\text{dist}(i, j)$  is the Euclidean distance between the positions of cells  $i$  and  $j$ . To optimize, we used a learning rate of 0.001 for 200 gradient descent steps with Adam optimizer. The weights of the gene network are not regularized, but the network is distilled by (1) removing all edges less than  $\epsilon = 0.5$  for the lattice and lobe networks and  $\epsilon = 0.2$  for the core-shell network, and (2) performing 3 iterations of a brute force process where each edge is removed if the resulting gene network creates a structure with a loss of at least 3800 (lattice network), 2300 (lobe network), or 2 (core-shell network).

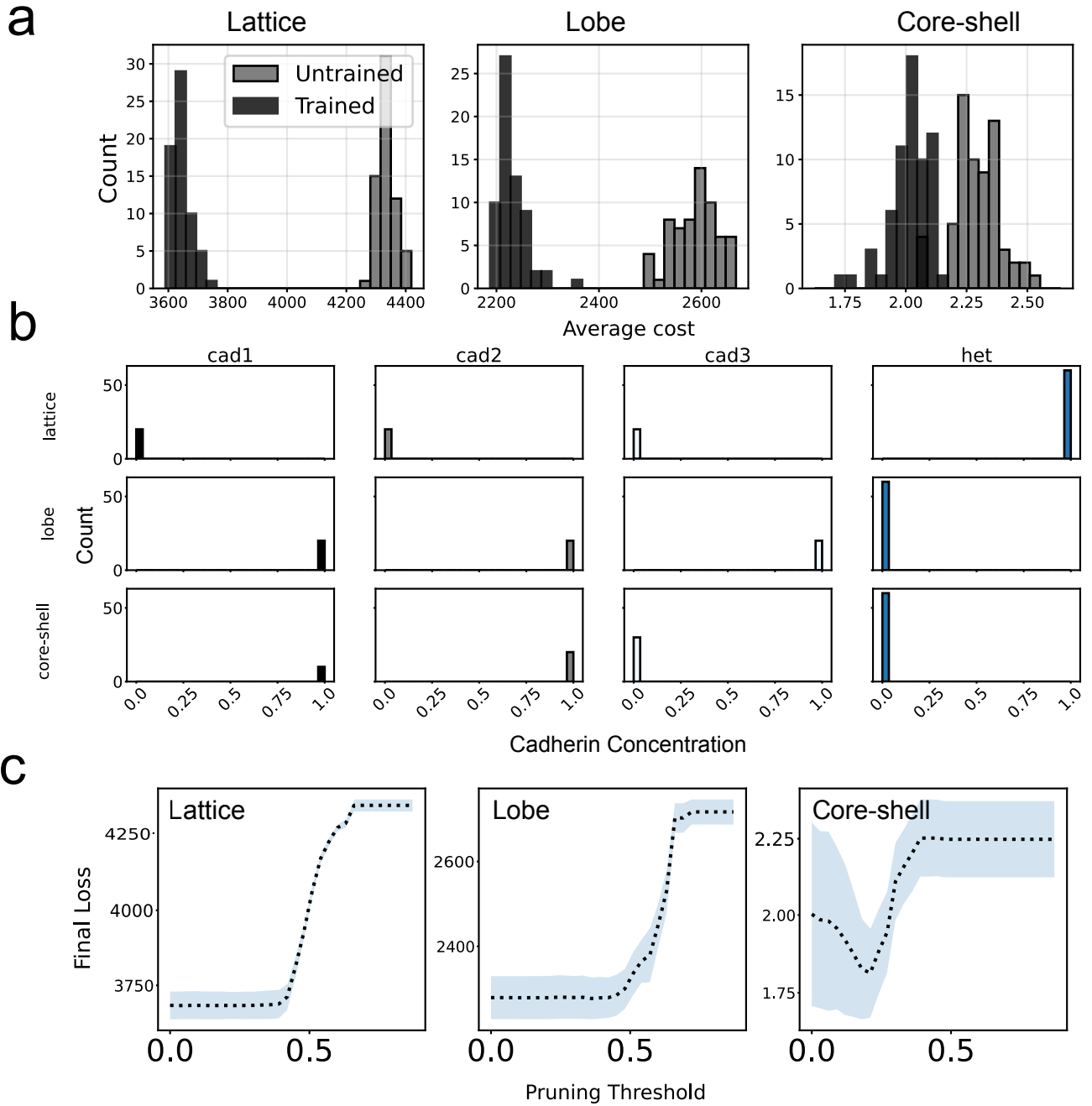


**FIG. S1. Chemical Regulation of Cellular Adhesion.** (a) Results of 64 forward simulations run with trained parameters compared to those with untrained parameters, for each of the three sorting problems (lattice, lobe and core-shell); the average cost over all time steps of each simulation is plotted. (b) Cadherin concentrations in final state of simulations run using trained parameters. For each sorting problem, a forward simulation is run using trained parameters. The concentrations of each cadherin type (homotypic cad1, cad2, cad3 and the heterotypic cadherin het) at the final time step are shown. As mentioned in the main text, simple mechanisms are learned where each cell simply up- or down- regulated its cell type specific cadherin, as well as the heterotypic cadherin. (c) Pruning plots for chemical adhesion gene networks. Plotted are the average and standard deviation of loss values for 30 simulations run with a gene network that has edges  $i$  pruning threshold set to zero. This is used to determine the best pruning thresholds to distill the learned gene networks.

### Elongation

The forward simulation is initialized with 1 cell in 3D, and run for 119 cell division steps. The simulation consists of 10 chemicals and 32 internal genes, and the gene network takes as input sensed chemical concentrations, chemical gradients, division propensities, and cell radii. Diffusion occurs in a closed system.

*Optimization.* The loss function is calculated as the sum of the squares of the z-coordinate of each cell; minimizing this forces the cluster to elongate vertically. Training is done on a batch of 4 simulations, and a batch of 4 simulations is used to evaluate the validation loss. We use a learning rate of 0.001 for 500 gradient descent steps with Adam optimizer. The weights of the learned gene network are L1-regularized with  $\lambda = .1$ . The weights of the gene network are initialized to values drawn from a normal distribution with  $\sigma = .1$ . The weights of the learned gene interaction matrix are pruned (set to zero) if they are below  $\epsilon = 0.9$ . This threshold is determined by pruning the learned parameters at various thresholds and measuring the loss of 50 simulations run with pruned parameters (Fig. IIIa).

### Branching

The simulation is initialized with 1 cell in 2D, and run for 129 cell division steps to generate a cluster of 130 cells. Simulations are done with 20 chemicals and 50 internal genes; the gene network takes as input sensed chemicals, chemical gradients, division propensities, and cell radii. Diffusion occurs with heuristic boundary conditions.

*Optimization.* The loss function is calculated by defining a shape mask that specifies the region of space cells should occupy to be rewarded. Cells that are within the mask are given a reward of 3.0 and cells that are not are given a penalty of -1. These values are summed over all cells and an asymmetry penalty is added to prevent cells from forming just one branch. The asymmetry penalty is given by the absolute value of the sum of the x-coordinates of cells. We use a learning rate of 0.01 for 400 gradient descent steps with Adam optimizer. The weights of the learned gene network are L1-regularized with  $\lambda = .1$ . The weights of the gene network are initialized to values drawn from a normal distribution with  $\sigma = .1$ .

*Regeneration.* To obtain the regeneration plot shown in the main text, forward simulations are run using optimized parameters. A fraction  $f$  of cells is removed by deleting  $f * N$  random indices, where  $N$  is the total number of cells in the structure, and a simulation is run for  $(1 - f) * N$  steps using the partial structure as the initial state. The final loss after regeneration is averaged for 15 simulations, for various  $f \in [0, 1]$ .

### Chemical Homeostasis

The simulation is initialized with 20 cells, and run for 100 cell division steps. The initial cells are divided into two cell types, where each cell type can only secrete one of two chemicals in the simulation. An initial imbalance between the two cell types is set by assigning 20% of the initial cells to be the first cell type and the remaining to be the second cell type. The simulation contains 8 internal genes, and the gene network takes as input sensed chemicals, division propensities and cell radii. Diffusion occurs in a closed system.

*Globally-shared Regulation.* The parameters of the regulatory network are shared by all cells in the simulation. The distinction between the two cell types is based on the ability of secreting one chemical and not the other, while both cell types can sense the concentration of both chemicals. This is the case reported in the main text.

*Cell Type Specific Regulation.* In this case each cell type is equipped with a different regulatory network, shared among all cells of the same type. Each cell type can still only secrete one chemical of the two but sense the concentration of both of them. Fig IIIa showcases gene networks for cell type 1 and 2 obtained from different optimization runs. Out of 20 optimization runs, 12 converged to the architectures in the top row, the other on one of the other two cases. Notice the consistency in the discovered architectures, especially of the stronger (bolder) connections. Fig IIIb schematically represents the model optimized in this context.

*Optimization.* The loss function is calculated as the imbalance in the number of cell types, given by:

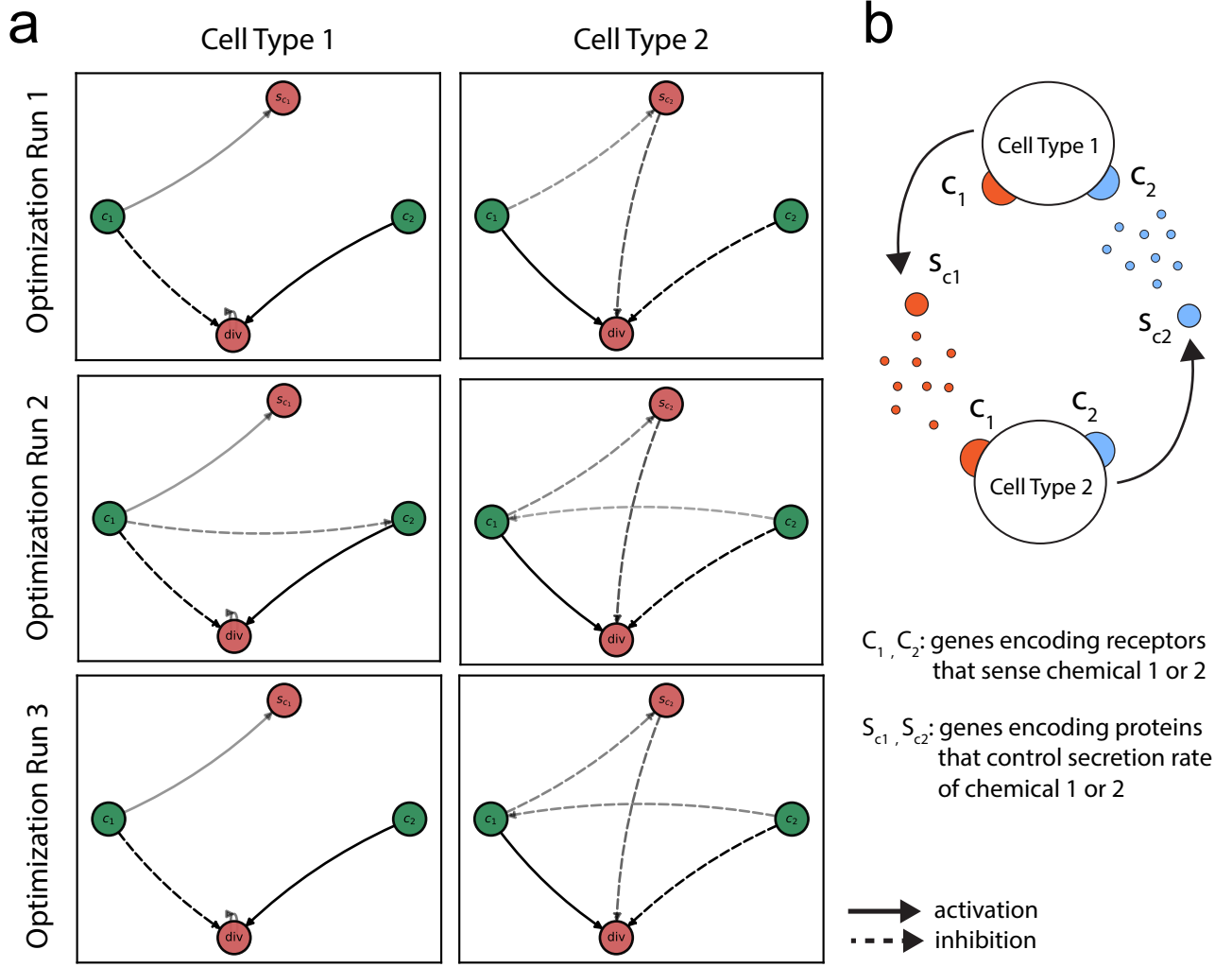


FIG. S2. **Chemical Regulation of Homeostasis with Cell Type Specific Networks.** (a) Gene network architectures for each cell type (on columns) obtained from different optimization runs (on rows). Green nodes are sensory inputs (i.e. sensed chemical concentrations, while red nodes are outputs (secretion of the cell type specific chemical and division probability). (b) Schematic representation of the model we optimize over.

$$\mathcal{L}_t = |\text{num type 1 cells} - \text{num type 2 cells}|$$

We used a learning rate of 0.01 for 400 gradient descent steps with Adam optimizer. The weights of the learned gene network are L1-regularized with  $\lambda = .1$ . To have the untrained state maintain the initial imbalance of the cell types in the generated structure, the weights of the gene network are initialized to very low values, resulting in a homogeneous division propensity that could only be broken by learning how to chemically regulate division to maintain equal numbers of cell types.

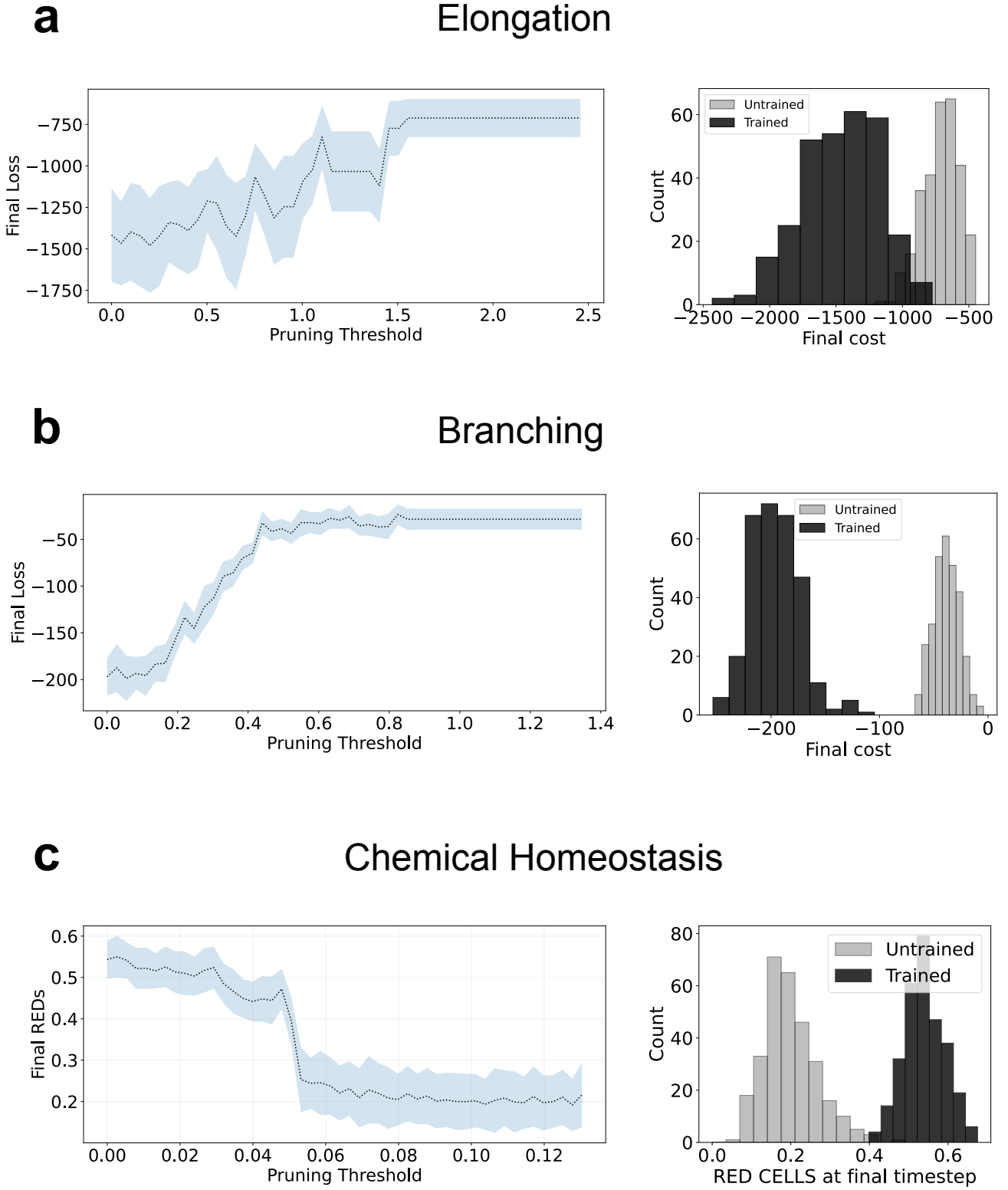


FIG. S3. **Elongation, Branching and Chemical Regulation of Homeostasis.** Final losses for a range of pruning thresholds shown on the left for gene network learned for (a) Elongation, (b) Branching, and (c) Chemical Homeostasis. Losses are averaged over 50 simulations, and shaded area shows one standard deviation. On the right, histograms comparing the distribution of final losses from the untrained and trained models for each of the three cases; there is a clear separation of the trained model from the untrained.

### Mechanical Control of Cell Proliferation

The forward simulation starts from one cell and is run for 200 time steps. Throughout the simulation, an external field is established over the cells to mimic the effect of a growth factor gradient. The value of the field scales as  $1/r^2$ , with  $r$  being the distance to the center of the cluster. At every cell division step, the division propensity calculated by the gene network is scaled by the value of this field:

$$d_i = d_i * \frac{1}{2 + 0.4 * r^2}$$

where  $d_i$  is the division propensity of cell  $i$ . This emulates the effect of a growth factor gradient - cells closer to the center are more likely to divide than cells closer to the edge. The simulation is run with 2 chemicals and 4 hidden genes, with the gene network being able to sense the cell's chemical concentration, chemical gradients, and mechanical stress. Mechanical relaxation occurs for a fewer number of steps in this simulation than in the other examples to prevent rearrangements from dissipating stress. Diffusion occurs with heuristic boundary conditions.

*Optimization.* Optimization is performed with a batch of 4 simulations for training, and a batch of 16 simulations for evaluation of the validation loss. We use a learning rate of 0.001 for 300 gradient descent steps with Adam optimizer. The weights of the learned gene network are L1-regularized with  $\lambda = .1$ . The loss function is the coefficient of variation of division propensities at the final time step. This optimization worked best without a REINFORCE gradient estimate - information from the last time step is enough to learn a mechanism. The weights of the gene network are initialized to zero so that the initial cluster grows as prescribed by the growth factor gradient.

To evaluate the nature of the learned mechanism, inputs to the trained model are ablated, by replacing the weights of the gene network corresponding to a specific input to zeros. In this way, we ablated chemicals, chemical gradients and stress as inputs, finding that ablating stress results in markedly decreased performance of the mechanism (Fig S4c). We additionally tested the learned mechanism on other kinds of fields (as described in the main text) and saw that the distribution of unscaled division propensities seem to match the distribution of stress buildup in the cluster (Fig S4d).



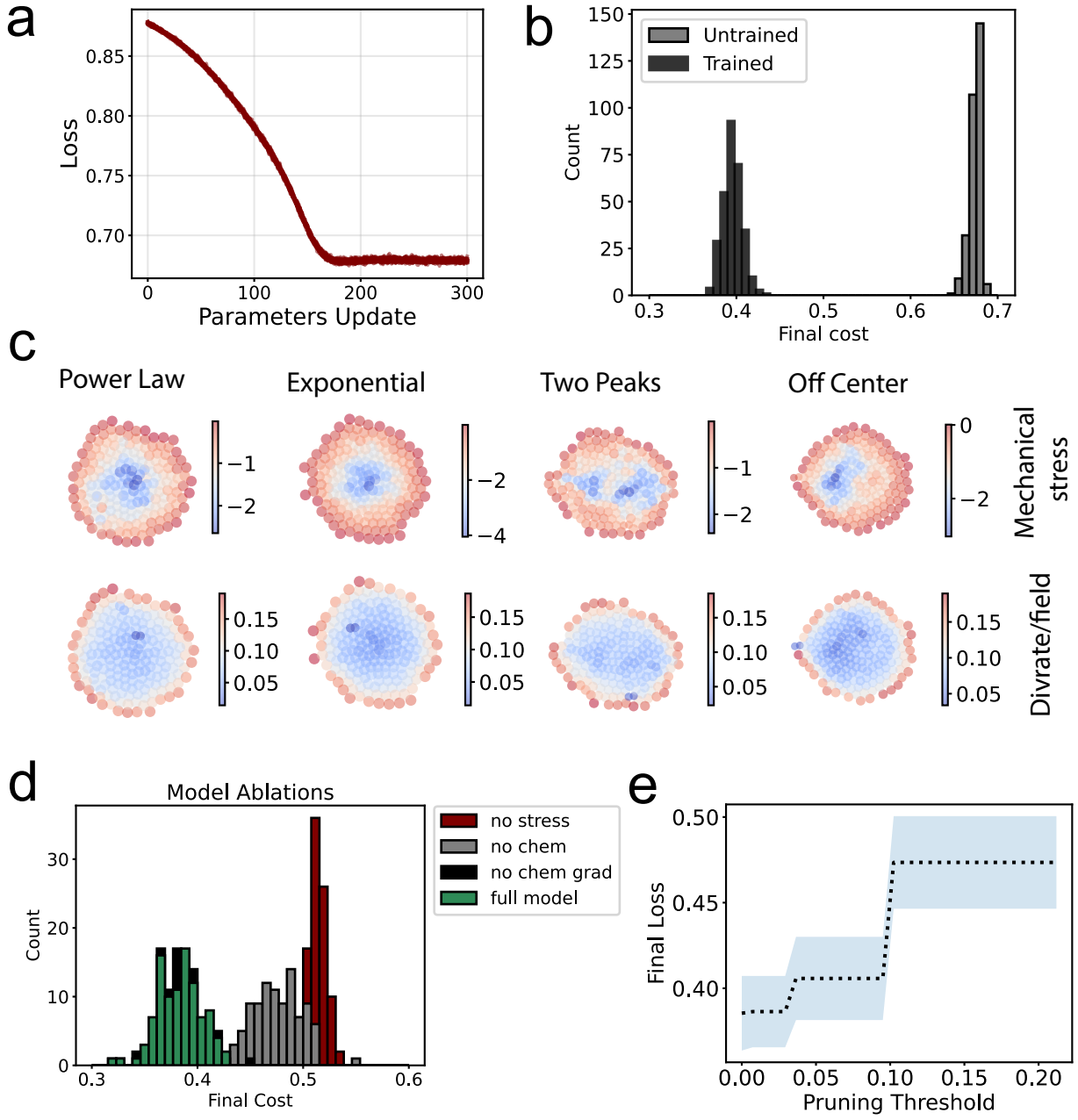


FIG. S4. **Mechanical Control of Cell Proliferation.** (a) Final costs of 300 forward simulations ran with trained parameters and untrained parameters. (b) Final costs of 300 forward simulations ran with trained parameters, ablating one of the input features to the gene network. Ablation is performed by setting outgoing edges from the desired feature to zero. Ablations show that mechanical stress is the most important feature used by the gene network to regulate division rates. (c) Visualizations of forward simulations run with trained parameters, but with a different shape of field than the one trained on. Top row shows the mechanical stress accumulation under different kinds of field, which follows the prescribed field. Bottom row shows the division rate unscaled by the field - the learned values weakly follow the pattern of stress accumulation. (d) Pruning plot showing final costs for various pruning thresholds of network weights.

#### IV. SCALING OF OPTIMIZATION PERFORMANCE WITH MODEL COMPLEXITY

Over-parametrized deep networks have shown a remarkable generalizability in learning target functions. In a similar vein, we preliminarily investigated how our optimization performance scales with the complexity of the regulatory network in our cells – i.e, the number of secreted morphogens and the number of interacting genes (Fig S5). We restrict ourselves for simplicity to the 2D case of growing elongated and branched structures. In learning the decision-making circuits required for cells to grow into a pre-specified shape (either an elongated cluster or a branched "V-shaped" structure), a lower validation loss is reached by increasing the number of morphogens each cell can locally communicate with. The rate of success of optimizations - the fraction of optimizations that are able to successfully create the desired shape - also increases with the number of morphogens. Without a sufficient number of morphogens, however, none of the optimizations can learn a successful decision-making network to create the desired shape. In the case of the V-shape, increasing the number of interacting genes did not have a pronounced effect. Interestingly, for the case of the elongated cluster, increasing the number of genes helped learn successful mechanisms in systems with low numbers of morphogens. In both cases, a sufficient number of both morphogens and genes is necessary to learn a successful mechanism. These findings indicate a minimal complexity required to build shapes and an interesting tradeoff between the quantity of communication signals (number of morphogens) versus the complexity of the local communication network (number of interacting genes).

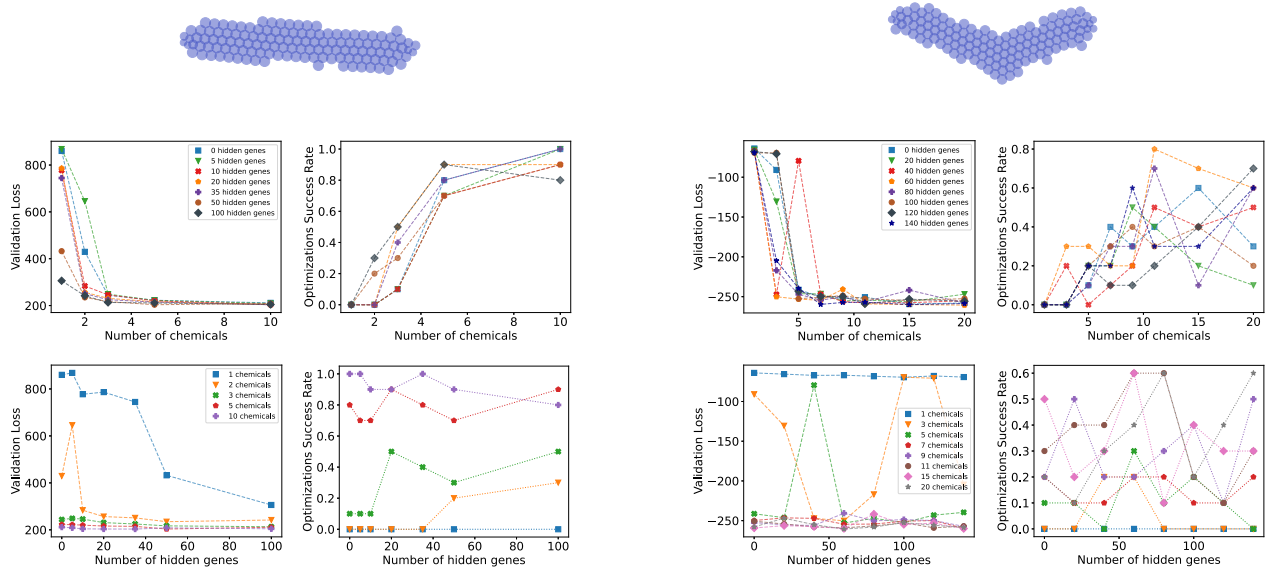


FIG. S5. **Scaling of Optimization Performance with Model Complexity.** (a) Scaling of validation loss and success rates for elongation. Losses are collected for 10 optimizations run from a different random seed for each condition. Training is done over 500 gradient descent steps and a batch of 8 simulations. (b) Scaling plots for V-shape case. Losses are collected for 10 optimizations run from a different random seed for each condition. Training is done over 300 gradient descent steps and a batch of 8 simulations.

TABLE I. Definition of Notation

Notation	Definition
$T$	number of timesteps
$N$	number of cells in final state
$n$	number of cells in initial state
$\text{Dim}$	dimension of cell property
$R$	cell radii
$N_c$	number of chemicals in system
$N_{\text{ctype}}$	number of celltypes in system
$N_t$	number of timesteps
$\bar{r}_i$	position of cell $i$
$d_i$	division propensity of cell $i$
$\bar{g}_i$	gene concentration vector of cell $i$
$c_k(\bar{r}_i)$	chemical $k$ concentration at position $\bar{r}_i$
$D$	diffusion coefficients
$S$	secretion rates
$K, k_i$	degradation rates
$W_{ij}$	interaction weight of gene $j$ regulating gene $i$
$I_i$	input signal to gene $i$